ARCHIVIO ISTITUZIONALE
DELLA RICERCA

Alma Mater Studiorum Università di Bologna
Archivio istituzionale della ricerca

Loss of Snord116 impacts lateral hypothalamus, sleep, and food-related behaviors

This is the final peer-reviewed author’s accepted manuscript (postprint) of the following publication:

Published Version:
Pace, M., Falappa, M., Freschi, A., Balzani, E., Berteotti, C., Lo Martire, V., et al. (2020). Loss of Snord116 impacts lateral hypothalamus, sleep, and food-related behaviors. JCI INSIGHT, 5(12), 1-17 [10.1172/jci.insight.137495].

Availability:
This version is available at: https://hdl.handle.net/11585/770438 since: 2024-05-10

Published:
DOI: http://doi.org/10.1172/jci.insight.137495

Terms of use:

Some rights reserved. The terms and conditions for the reuse of this version of the manuscript are specified in the publishing policy. For all terms of use and more information see the publisher's website.

This item was downloaded from IRIS Università di Bologna (https://cris.unibo.it/).
When citing, please refer to the published version.

(Article begins on next page)

14 January 2025

Loss of *Snord116*, sleep and food-related behaviors: a report of changes in lateral hypothalamus

Marta Pace [1#], Matteo Falappa [1,2#], Andrea Freschi[1], Edoardo Balzani[1], Chiara Berteotti[3], Viviana Lo Martire[3], Fatemeh Kaveh [4], Eivind Hovig [4,5], Giovanna Zoccoli [3], Roberto Amici [6], Matteo Cerri [6], Alfonso Urbanucci [4], Valter Tucci *[1]

[1] Genetics and Epigenetics of Behaviour Laboratory, Istituto Italiano di Tecnologia, via Morego 30, 16163, Italy.
[2] Dipartimento di Neuroscienze, Riabilitazione, Oftalmologia, Genetica e Scienze Materno-Infantili (DINOGMI), Università degli Studi di Genova, Genova, Italy;
[3] PRISM Lab, Department of Biomedical and Neuromotor Sciences, University of Bologna, Bologna, Italy
[4] Department of Tumor Biology, Institute for Cancer Research, Oslo University Hospital, Oslo Norway
[5] Centre for Bioinformatics, Department of Informatics, University of Oslo, Oslo, Norway
[6] Department of Biomedical and NeuroMotor Sciences, Alma Mater Studiorum - University of Bologna, Bologna, Italy;

[#] These authors contributed equally

* corresponding author:

Valter Tucci, Ph.D.
Senior Group Leader
Neurobehavioural Genetics Group
NBT – IIT Via Morego 30,
16163, Genova -- Italy
email: valter.tucci@iit.it

General information:

Abstract words: 186; words count: 11975 figures: 4; Supplementary material: figures 6; table 8

Conflict of Interest: each author discloses the absence of any conflicts of interest relative to the research covered in the submitted manuscript.

Abstract

Imprinted genes are highly expressed in the hypothalamus; however, whether specific imprinted genes affect hypothalamic neuromodulators and their functions is unknown. It has been suggested that Prader-Willi syndrome (PWS), a neurodevelopmental disorder caused by lack of paternal expression at chromosome 15q11-q13, is characterized by hypothalamic insufficiency. Here, we investigate the role of the paternally expressed *Snord116* gene within the context of sleep and metabolic abnormalities of PWS, and we report a significant role of this imprinted gene in the function and organization of the two main neuromodulatory systems of the lateral hypothalamus (LH), namely, the orexin (OX) and melanin concentrating hormone (MCH) systems. We observe that the dynamics between neuronal discharge in the LH and the sleep-wake states of mice with paternal deletion of *Snord116* (PWScr$^{m+/p-}$) are compromised. This abnormal state-dependent neuronal activity is paralleled by a significant reduction in OX neurons in the LH of mutants. Therefore, we propose that an imbalance between OX- and MCH-expressing neurons in the LH of mutants reflects a series of deficits manifested in the PWS, such as dysregulation of rapid eye movement (REM) sleep, food intake and temperature control.

Key words

Prader Willi syndrome, (PWS) REM sleep, Orexin/Hypocretin, Melanin concentrating hormone, hypothalamus, Paternally expressed genes (PEG3)

Founding

This study was financially supported by Jerome Lejeune Foundation under Grant Agreements No 1599-TV2016B, by the The Foundation for Prader Willi Research, this project received the Seal of Excellence by the European Union’s Horizon 2020, N 753417. AU was financially supported by the Norwegian Cancer Society (Grant number 198016-2018).

Introduction:

Both maternally and paternally derived genes are essential for survival beyond post-fertilization; these genes differentially affect embryonic brain development and, consequently, postnatal and adult physiology. In particular, paternally derived genes are thought to control the organization of the subcortical limbic system [1]. For example, androgenetic (two paternal copies) cells are mainly distributed in the hypothalamus, although the specific impact of such parental genetic information on hypothalamic functions remains unknown.

The hypothalamus is an ancient structure that orchestrates primitive physiological processes for survival [2], such as motivated behaviors for feeding and drinking, the regulation of body temperature and the switch between sleep and wakefulness. Therefore, a number of paternally expressed genes and overlapping circuitries in the hypothalamus function as potential regulators of mammalian sleep and sleep-mediated metabolism [3]. To this end, over the last decade, we have demonstrated that parent-of-origin imprinted genes exert a pivotal role in the control of sleep physiology and feeding behavior [3, 4]

Among the pathological conditions that depend on genomic imprinting defects, Prader–Willi syndrome (PWS) is the neurodevelopmental disorder that, up to now, best describes the link among sleep, metabolism and imprinted genes. PWS results from the loss of a cluster of paternally expressed genes on the chromosome 15q11-q13 region, many of which are highly expressed in the hypothalamus and are characterized by sleep-wake (e.g., rapid-eye-movement, REM, alterations) and metabolic (e.g., hyperphagia) abnormalities. All these symptoms are generally associated with hypothalamic insufficiency [5-7].

We have previously described that microdeletion of the small nuclear ribonucleic acid (RNA)-116 (*SNORD116*) cluster within the PWS locus induces REM and temperature dysregulations in mice and human subjects [5]. Specifically, the deletion of *Snord116* in mice causes an EEG profile characterized by the intrusion of REM sleep episodes into the transition between wakefulness and sleep accompanied by an increase in body temperature. REM sleep intrusions have been reported in several clinical studies in which PWS subjects manifest narcolepsy and express symptoms such as sleep attacks during active wakefulness, cataplexy (a transient loss of muscle tone during wakefulness), sleep paralysis and sleep fragmentation [8]. Narcolepsy is a sleep condition that causes the loss of hypothalamic OX neurons (also known as hypocretin; HCRT)[9], and previous studies have observed that subjects with PWS show OX alterations [10-12].

OX neurons are located in the lateral hypothalamus (LH), where this class of neurons promotes wakefulness [13] by facilitating the release of other arousal-promoting brain neuromodulators (i.e., noradrenaline, histamine and acetylcholine) [14]. However, in the LH, OX neurons are intermingled with a group of neurons that release the melanin-concentrating hormone (MCH) and promote sleep, and these neurons are active mainly during REM sleep [15]. Both OX and MCH neurons project widely throughout the brain, exerting antagonistic actions on brain states and energy balance. However, whether these two groups of neurons of the LH exert abnormal control over sleep-wake cycles, feeding and temperature in the PWS remains unclear.

In this study, we tested the hypothesis that the loss of paternally expressed *Snord116* disrupts specific neuromodulatory systems of LH, particularly those that overlap in the control of sleep, feeding and temperature. We found that mice with paternal deletion of *Snord116* have altered dynamics in how neuronal activity of the LH is associated with sleep-wake cortical states and feeding. This altered modulation between cortical states, behavior and subcortical neuronal activity in *Snord116*-deleted mice is accompanied by a loss of OX-expressing neurons in the LH. We also report, for the first time, a link between *Snord116* and a different paternally imprinted gene, *Peg3*, which has been recently associated with the control of the hypothalamic OX neuromodulatory system [16].

Results:

Loss of paternal *Snord116* alters neuronal dynamics in the LH associated with sleep homeostasis

To investigate whether the firing pattern of neurons within the LH manifests signs of paternal-dependent subcortical regulation throughout different arousal states of the brain, we studied mice with paternal deletion of the *Snord116* gene [17], PWScr$^{m+/p-}$ mice, and their wild-type littermate controls, PWScr$^{m+/p+}$ mice. A total of 569 well-sorted units were successfully recorded from PWScr$^{m+/p+}$ wild-type mice, and 548 units were recorded from PWScr$^{m+/p-}$ mutant mice across all time points. Based on the distribution of the firing activity of each unit, we were able to distinguish populations of putative neurons in the LH that were time-locked with the occurrence of specific sleep-wake states (Figures 1C and 1E). In particular, we identified neurons (Figure 1E) associated with sleep (S-max) or wakefulness (W-max). However, we distinguished between NREM (NR-max), REM (R-max) neurons and neurons firing in both stages (NRR-max) (Table S1). We also identified a group of neurons that did not show significant changes in their firing rate across the sleep-wake states, and we called this latter class of neurons "ws" (wake and sleep).

Next, we identified LH neurons that are time-locked to food intake. In this experiment, a total of 147 units were identified from PWScr$^{m+/p+}$ mice and 74 units from the PWScr$^{m+/p-}$ mice in response to food deprivation. Neurons were classified as Type I (*i.e.*, fire maximally after nose-poking/feeding activity), Type II (*i.e.*, fire maximally before nose-poking/feeding activity) and Type III neurons (*i.e.*, not-responding neurons).

Strikingly, we observed a significant increase in S-max and a reduction in W-max neurons in PWScr$^{m+/p-}$ mutant mice compared with controls at baseline (Figure 1G and Table S2). A more detailed analysis of the baseline (*i.e.*, B1 and B2, as shown in Figure 1G) confirmed this distribution of the classes of LH neurons according to EEG states (Figure S1B and Table S2). Moreover, when the pressure of sleep is low (*i.e.*, B1), mutant mice exhibit more REM sleep than their littermate controls (Figure S1A). This finding suggests that the pressure/need of sleep may be either a permissive or a blocking mechanism with respect to excess REM sleep due to the lack of *Snord116*. This phenomenon is confirmed by the profile of the power densities in REM sleep (Figure S1C). Indeed, in PWScr$^{m+/p-}$ mutant mice, the theta (4.5-9 Hz) band, which is characteristic of REM sleep, is higher in both B1 and B2, but at B2, the EEG frequency phenotype is not accompanied by longer REM sleep duration, implying that the overall higher sleep pressure masks differences in microstructural aspects of electrophysiological sleep. Moreover, the delta (0.5-4.5 Hz) band presents an opposite trend in the two groups of animals; counterintuitively, reduced power is observed in mutant mice as the pressure of sleep increases (Figure S1C). Again, this phenomenon suggests abnormal homeostatic control of sleep in mutant mice.

Thus, we sought to explore the physiological responses of mice following 6-h of total sleep deprivation (SD) by investigating the distributions of the neuronal classes at different time points during 18 h of recovery (i.e., SD1, SD2 and SD3, Figure 1B). We observed that SD induced an increase in S-max neurons in wild-type PWScr$^{m+/p+}$ mice, while in mutant PWScr$^{m+/p-}$ mice, the distribution of classes of neurons remained unaltered compared with baseline (Figure 1G). This result indicates that control mice homeostatically respond to SD by modulating LH neuronal dynamics, as previously reported in the literature [18], while mutant mice lack this hypothalamic modulatory process.

Across different conditions, neurons may continue responding to the same state, may respond to different state, or may become aspecific in their activity. Within the rearrangements of neuronal modulation across different phases, an interesting observation in our study is represented by the behavior of the non-responding neurons following SD (Figure S1A, Table S3). In wild-type mice after SD, the number of neurons of this latter class increases three times compared with the previous baseline, a phenomenon that is gradually recovered over the following 18-h after deprivation. This change comes with a cost for wake-dependent neurons in wild-type animals. In PWScr$^{m+/p-}$ mutants, this SD effect is missing, reinforcing the observation of a lack of neuromodulation caused by the paternally derived genetic defect.

Finally, the dramatic drop in delta and theta power densities in PWScr$^{m+/p-}$ mutant mice compared with controls at SD2 (Figure S1C) coincides with the permissive role of sleep pressure at this time of the day for the sleep defects in mutants.

The LH is made up of a heterogeneous group of cells that express various neuropeptides, such as OX and MCH neurons. To gain insight about the heterogeneous nature of our recording units, we plotted the mean firing rate versus the mean logarithm of the EMG signals across three groups of putative neurons (W-max; S-max and ws neurons) of the whole sleep experiment (Figure S1D). The graphical representation of these neurons within the 2D scatter plot enables us to distinguish between MCH putative and OX putative neurons. MCH putative neurons fire maximally during REM sleep and are thought to present a low EMG amplitude and a low average discharge rate of 1.1 ± 0.26 Hz, while OX putative neurons fire maximally during wake and are characterized by a high firing rate, 3.17 ± 0.79 Hz, as both classes of neurons were previously described [19]. Based on these criteria, we assessed MCH putative and OX putative neurons between PWScr$^{m+/p+}$ wild-type and PWScr$^{m+/p-}$ mutant mice. The percentage of recorded MCH putative neurons was unchanged between the two genotypes; although non-statistically significant, a total of 211 OX putative neurons were identified in PWScr$^{m+/p-}$ mutant mice compared with 315 OX putative neurons identified in control mice (Figure S1D).

A high proportion of neurons in the LH do not respond to food intake in PWScr$^{m+/p-}$ mutant mice

Mice underwent food deprivation (FD) during the dark period/resting phase (Figure 1B) to increase their drive for food intake. When food was made available again, pellets were automatically provided in the home cages of each mouse (see Methods). The frequency of nose-poke activity to gain food was similar between the two genotypes (PWScr$^{m+/p-}$: 107 trials; PWScr$^{m+/p+}$: 116 trials), indicating no obvious behavioral differences between the two genotypes, as previously described [20, 21].

As for the sleep experiment, our attention fell on the distribution of neuronal modulation between the two genotypes. We found that PWScr$^{m+/p-}$ mutant mice had less than half the number of type II neurons, which have reduced firing during food intake, of control mice (Figure 1G). This reduction may be explained by the fact that mutant mice had twice as many non-responding neurons as control mice. Indeed, type I neurons were almost identical in the two groups (Table S4). These results also suggest for an abnormal distribution of OX neurons in the LH of mutants, as OX neurons drive food intake.

Sleep homeostasis is disrupted in PWS mutant mice

We explored the 24-h EEG profile of sleep (see Methods) and the responses to sleep loss in a different cohort of animals.

The results confirmed our previous observations that sleep is altered in the PWS mutants [5]. In particular, REM sleep is increased in PWScr$^{m+/p-}$ mutants compared with controls, showing a peak increase at ZT (Zeitgeber Time) 20 and an overall increase in theta power (Figure 2A). These experiments were conducted at standard room temperature of 22°C. Interestingly, the theta profile in mutants did not show circadian rhythm (Figure 2A); PWScr$^{m+/p-}$ mutants had an increase in theta power during the transition between light and dark, when the pressure of sleep is low. Overall, REM sleep abnormalities remained a selective phenotype in these mutants, while the other EEG-determined arousal states were unchanged between the two genotypes (Figure S2A).

Moreover, we tested for the first time the homeostatic EEG response following SD in PWScr$^{m+/p-}$ mutant mice compared with littermate controls. Compared with control mice, PWScr$^{m+/p-}$ mice showed reduced delta activity during non-REM (NREM) sleep rebound following SD (Figure 2B), although the total amount of NREM sleep was unaltered over the long-term recovery process (Figure S2A). Notably, delta power is the best electrophysiological marker of sleep propensity, although the temporal distribution of its rebound following SD is less characterized. The behavior of delta sleep in mutant mice suggests a dysregulation in the daily distribution of sleep pressure in these mice.

Our results also showed a significant decrease in REM sleep during the first 2-h of rebound in mutants compared with controls (Figure 2A), confirming both the alteration of homeostatic control in mutants and the alteration of REM sleep.

Thermoneutrality does not increase REM sleep in mutants

REM sleep is an evolutionarily recent physiological state of sleep that, in mammals, is largely dependent on the environmental temperature [22, 23]. The maximum REM sleep expression in mice is attained when the environmental temperature is near 29°C. The latter represents a thermoneutral zone (TNZ) for this species [24]. In a new set of experiments, we modified the temperature environment of the animals to allow the duration of REM sleep to reach a maximum [24]. Mice were housed for 5 weeks at 30°C, and then, EEG/EMG were recorded for 24-h at the TNZ.

We observed that PWScr$^{m+/p-}$ mice showed a significant increase in the distribution of sleep stages (*i.e.,* total sleep, NREM and REM sleep) at 30°C during the dark period at ZT 20, which in mice account for high sleep pressure [25, 26]. This data suggests that the TNZ facilitate the accumulation of sleep pressure during the active period (dark period) in the mutant mice (Figure 2A and S2A). The NREM sleep delta power and the REM sleep theta power were unchanged between the two genotypes, (Figure S2C and S2D).

Peripheral thermoregulatory responses are absent in PWS mutants

We tested whether loss of paternally expressed *Snord116* affects peripheral responses and whether these changes impact the overall body temperature and body weight of the animals. We monitored the peripheral and cutaneous body temperature at the head (T-head) and tail (T-tail), and consequently, we derived the heat loss index (HLI) (see Methods in the supplementary materials). Recordings were made at room temperatures of both 22°C and 29-30°C (TNZ). The TNZ imposes body temperature adjustments by changing the vasomotor tone in specialized heat exchange organs, such as the tail, in mice [27]. We observed an increase in the vasculature tail skin tone at the TNZ in both genotypes compared with 22°C (Figure 2C, upper panel). However, greater tail vasodilatation was observed in control mice, particularly between the switch from light to dark periods. These results indicate that while at TNZ, wild-type control mice present a proper peripheral thermoregulatory response when the pressure of sleep is low, which is instrumental in maintaining the core body temperature of the animal at this time of the day, mutant mice lack such an important physiological response. A significant increase in the HLI was recorded in both genotypes, but a greater increase was found in PWScr$^{m+/p+}$ wild-type mice than in mutant mice (Figure 2C, middle panel). We also observed that the peripheral body temperature recorded at 22°C increased in PWScr$^{m+/p-}$ mutant mice compared with control mice during the light period (Figure 2C, bottom panel), suggesting a diminished homeostatic control when sleep is physiologically facilitated in mice. Moreover, mutant mice failed to show the circadian oscillatory profile of temperature at RT that is present in PWScr$^{m+/p+}$ mice. However, at TNZ, the difference between the two genotypes during the light period was no longer observed. Furthermore, in agreement with previous reports [21], we observed that PWScr$^{m+/p-}$ mutant mice had a smaller body size when kept either at 22°C and at 30°C later in their development (*e.g.*, for only 5 weeks) and when they were exposed at 30°C from birth and kept at this temperature for up to 20 weeks of age (Figure S3).

Lack of *Snord116* impairs the OX system in the LH

To assess the regulation of the main neuropeptides in the LH, we examined the expression of OX and MCH. Thus, we assessed the precursor of MCH (*Pmch*) and the prepro-OX (*Ppox*). We examined three conditions (Figure S4A): at ZT 6, we tested both the baseline condition (T0) and the effects of SD (T1); and at ZT 7, 1-h after SD (T2), we tested the effects during the recovery from the loss of sleep.

We report that PWScr$^{m+/p-}$ mutant mice showed a significant increase in *Ppox* at T0 baseline compared with control mice, while *Pmch* was unchanged in both genotypes at T0 (Figure 2D). At T1, both *Ppox* and *Pmch* were significantly reduced in PWScr$^{m+/p-}$ mice compared with control mice (Figure S4B), confirming that the homeostatic response in mutants is reduced and that these two systems are dysregulated in mutant mice. At T2, the difference between the two genotypes for *Ppox* and *Pmch* was repristinated (Figure S4B), confirming that the effects of SD in mutants are only acute and follow the immediate response after sleep deprivation.

Then, we evaluated the receptors for MCH and OX. We assessed mRNA levels of OX receptor-1 (*Ox1R*) OX receptor-2 (*Ox2R*) and MCH receptor 1 (*Mch1R*) in the hypothalamus and in other brain areas as control measures. The expression levels were overall unchanged between the two genotypes, except for *Ox2R* in the parietal cortex (Figure S4C).

The overall contrast between neuropeptides and the mRNA levels of their receptors prompted us to quantify whether these chemical changes within the OX and MCH systems had consequences for the organization of the neuronal populations of the LH. We observed a significant reduction in OX neurons in the LH of PWScr$^{m+/p-}$ mutant mice (PWScr$^{m+/p+}$ mice 95 ± 9; PWScr$^{m+/p-}$ mice 53 ± 10; p= .0005; Figure 2E), while MCH neurons, which are located near the OX neurons, were unaffected (PWScr$^{m+/p+}$ mice 66 ± 5; PWScr$^{m+/p-}$ mice 63 ± 5; Figure 2E). The discrepancy between the increased *Ppox* and the reduced neuronal population may be due to a mechanism to compensate for the low number of neurons with an overproduction of the peptide, as it has been already described in *Magel2* knockout mice, which account for another mice model of PWS [28].

Loss of *Snord116* leads to transcriptional reprogramming in the hypothalamus

Next, we investigated whether the loss of *Snord116* affects overall gene expression in the whole hypothalamus of PWScr$^{m+/p–}$ mutant mice compared with PWScr$^{m+/p+}$ control mice by performing RNA sequencing (RNA-seq). The mice were investigated at the beginning of the light period ZT 0 (group 1, G1), 6-h later at ZT 6 (group 2, G2) and at ZT 6 but following 6-h of SD (group 3, G3). First, we sought to identify the differentially expressed genes (DEGs) between the two genotypes in the G1 group. We identified 4777 downregulated genes and 4271 upregulated genes between genotypes (adjusted $p < 0.05$; see Methods) and a minimum fold change of 2 (Table S8). Next, we compared the down- and upregulated DEGs (Figure 3 A-B) in G1 PWScr$^{m+/p-}$ mutant mice with DEGs derived from post-mortem hypothalamic data from PWS patients vs healthy controls [29]. Approximately 40% of mice DEGs overlapped with human DEGs, suggesting that loss of *Snord116* recapitulates approximately 40% of the transcriptional changes found in the human hypothalamus (Figure 3 A-B; Hypergeometric test p= 5.308548e-12). To more closely evaluate the functional importance of these overlapping DEGs, we performed gene ontology (GO) enrichment analysis using Metascape [30]. We found enrichment of several biological processes important for normal neural functions among the downregulated DEG genes, while inflammatory systems were the processes significantly enriched among the upregulated DEGs (Figure 3A-B).

Interestingly, we found that *Ppox* was significantly downregulated in PWScr$^{m+/p-}$ mutant mice and in human PWS patients (Figure 3C), confirming that OX is involved in the abnormal regulation of REM sleep in PWS.

Next, we focused on how SD affects gene expression in the hypothalamus in both normal and PWScr$^{m+/p-}$ mutant mice. We compared DEGs in G2 versus G3 of each genotype (Figure 3D). We found that 6 h of SD largely influenced the transcriptome of mutant mice (i.e., 833 DEGs) compared with control mice (i.e., 30 DEGs). Surprisingly, in the mutant dataset, most of the DEGs were downregulated (804 genes downregulated vs 29 upregulated). GO analysis of all 833 DEGs revealed enrichment of cell organization, development and growth-related processes (Figure 3E), indicating that poor sleep negatively impacts the hypothalamus in PWS subjects, suggesting a clinical implication of these results. Finally, we investigated the RNA-seq dataset to determine whether *Snord116* loss significantly affects the expression of imprinted genes in humans and mice (refer to Table S9). Maternally expressed imprinted genes, such as *Meg3*, *Gnas*, and *H19*, as well as paternally expressed imprinted genes, such as *Nap1l5* and *Peg3*, were differentially expressed in mutant mice before and after SD (Figure 3F).

OX regulation in the hypothalamus depends on two paternally expressed genes, *Snord116* and *Peg3*

We next sought to confirm selected physiologically relevant DEGs identified within the RNA sequencing dataset by qRT-PCR. Among maternally and paternally imprinted genes that were altered in the hypothalamus of PWScr$^{m+/p-}$ mutant mice, we confirmed that *Peg3* showed a remarkable increase in expression in PWScr$^{m+/p-}$ mice (Figure 4A) compared with the control mice (Figure S5A). PEG3 binds to DNA based on its multiple zinc finger motifs and nuclear localization [31, 32]. Interestingly, a recent study found an association between *Peg3* and OX expression [16]. However, whether PEG3 is able to bind and regulate the expression of OX in living mice remains unclear. We noticed that two conserved promoter regions within a 3.2-kb fragment located upstream of the *Ppox* gene (Figure S5F) target specific expression within the LH [33]. We showed that PEG3 binds one of these regions. Specifically, chromatin immunoprecipitation [34] followed by quantitative real-time PCR (ChIP qRT-PCR, and Figure 4A) revealed that PEG3 binds the 2.5 kb OX regulatory element region in the hypothalamic mouse brain. Interestingly, a significant reduction in PEG3 binding was observed in PWScr$^{m+/p-}$ mice (Figure 4A), which may be associated with a significant reduction in OX-expressing neurons in mutant mice. Our results show that PEG3 positively regulates the expression of *Ppox* by enhancing its expression, as indicated by the presence of a strong enrichment of the H3K4me2/3 in the same region (Figure 4A). Conversely, H3K27me3, which is a marker of condensed chromatin [35], showed no enrichment in either genotype. The *Gapdh* promoter was used as a negative control for the ChIP experiment (Figure S5E). These data reinforce the evidence that PEG3 contributes to the regulation of *Ppox* by enhancing its expression (Figure 4A).

Then, we sought to investigate whether *Peg3* or *Snord116* plays any causal role in the regulation and formation of OX neurons, and we assessed the expression of these two genes in OX-deficient mice. Specifically, we used two genetic mouse models of OX deficiency, *Ppox* knockout (KO) mice [9] and OX neuron-ablated (ataxin-3 [Atx]) mice [36] (Figure 4B).

Atx mice selectively degenerate postnatally, and a loss of 99% of neurons or more occurs by the age of 4 months [36]. Therefore, in Atx mice, not only are OX neurons ablated, but co-transmitters are also eliminated [37]. Conversely, KO mice are only deficient in *Ppox* (Figure 4B).

Interestingly, we observed that *Peg3* was significantly increased in Atx mice compared with KO mice (p= .03). Moreover, *Snord116* was also increased in Atx mice compared with KO mice and control mice (p= .03; Figure 4B). Other imprinted genes tested were unchanged between genotypes (Figure S5B). These data suggest that dysregulation of both *Snord116* and *Peg3* are important and associated with the physiological maintenance of OX neurons. Indeed, we observed that both genes were significantly altered only in narcoleptic mice, in which OX neurons and their co-transmitters were ablated, but not in narcoleptic mice lacking only Ppox.

Finally, to test whether the alteration of *Peg3* observed in the PWScr$^{m+/p-}$ mice and in the Atx mice is linked to the absence of *Snord116* and whether *Snord116* modulates the expression of *Peg3*, we used an RNA-interfering approach aimed at silencing *Snord116* in immortalized embryonic rat hypothalamus cells (embryonic rat hypothalamus cell line R7). Specifically, cells transfected with a *Snord116*-specific siRNA showed significant *Snord116* inhibition of approximately 80% at 48 h after transfection (Figure 4C). However, the levels of *Peg3* were unchanged (Figure 4C), indicating that *Snord116* does not directly regulate the expression of the *Peg3* gene. *Pmch* and *Snurp* were also unchanged (Figure S5).

Discussion

Overall, this study shows evidence suggesting that *Snord116* plays a crucial role in the regulation of REM sleep and thermoregulation, both phenotypes being dysregulated in PWScr$^{m+/p-}$ mutant mice and patients [5, 38]. The mouse model we studied here, however, carries also a partial deletion of the *Ipw*, who may contribute to the effects we reported. In particular, we observed REM sleep alterations at a particular time of the day when the pressure of sleep increases [25, 26]; in mice, this occurs at a time in the sleep-wake cycle that corresponds to the "*siesta time*" [25, 26]. This phenomenon has the potential to help future experimental designs aimed at addressing temporally precise therapy.

Snord116 is one of the most important candidate genes involved in the aetiology of the major endophenotypes of PWS. Individuals lacking the *SNORD116* snoRNA cluster and the *IPW* (Imprinted In Prader–Willi Syndrome) gene suffer the same characteristics of failure to thrive, hypotonia, and hyperphagia that are observed in subjects with larger deletions and maternal uniparental disomy [39, 40]. However, the *Snord116* mouse model recapitulates all the sleep deficits of human PWS, but only incompletely mimics the metabolic alterations. Indeed, both PWS mice and human patients show an alteration of body weight, but the two species show opposite phenotypes; indeed, PWS patients exhibit increased body weight, while mouse models across different studies show reduced weight [21, 41], displaying at least only the first stage (Stage I) of the PWS clinical features, the infancy stage [42]. This overall result suggests that evolutionary divergency between the two species may have played an important role in the metabolism of PWS, but to date, there is no evidence for such a change.

We report for the first time an effect of the LH in *Snord116* mutant mice, which is accompanied by an imbalance between OX and MCH neurons, causing a 60% reduction in OX neurons in the LH, while MCH neurons were unaffected. Within the same 15q11-q13 region, it was previously reported that *Magel2* KO mice lose 40% of OX neurons [28]. These results suggest that multiple paternally expressed genes within the PWS region regulate the OX system in the LH, most likely in a dose-dependent manner. At baseline, we observed that fire discharge of neurons associated with sleep (*i.e.*, S-max neurons) are higher in mutant mice than in controls, suggesting that the role of *Snord116* that originates from the LH is important in the determination of abnormal sleep in PWS. Indeed, several lines of evidence indicate that LH exerts pivotal role in controlling the transition between sleep and wakefulness [15]. Furthermore, while we observed that the proportion of S-max and W-max neurons significantly changed after 6 h of SD with an increase in sleep neurons of approximately 13% in wild-type control mice, PWS mutants lack this neuronal response by the LH to sleep loss. In the LH, OX and MCH systems exert opposing effects on REM sleep [43]: OX suppresses while MCH promotes REM sleep. Therefore, the imbalance between OX and MCH systems in PWS mutants is in agreement with an increase in REM sleep.

Additionally, OX and MCH neurons in the LH regulate food intake and metabolism [44, 45]. We found that mutant mice displayed a higher proportion of neurons, which were classified as non-responding neurons (type III), relative to food intake than controls. In contrast, type II neurons, which are downregulated in the LH during eating, were significantly reduced in mutants. It has been demonstrated that OX neurons decrease their firing during eating and remain in a depressed state throughout the entire eating phase [46]. These findings suggest a lack of regulatory feedback mechanisms mediated by the OX system in relation to food intake in the LH of PWS model mice, a phenomenon that can relate to the hyperphagia and obesity phenotype observed in PWS patients. This evidence of neuromodulatory dysregulation of the LH is in agreement with previous results [20], which describe that a late onset of mild hyperphagia and obesity in mice can be induced only when *Snord116* is selectively disrupted in the hypothalamus in adult mice.

Dysregulation of the OX system has been reported in a few clinical studies, although to date, the results remain contradictory. One study described an increase in the OX-A level in PWS subjects [47], while another showed a decrease in the peptide in the cerebrospinal fluid [11]. Taken together, these findings call for an alteration of the OX system in PWS, although the contrasting results may also suggest that the loss of function of paternal alleles within the PWS region results in an increased phenotypic variance.

Our data suggest also that *Snord116* is involved in the regulation, formation and maintenance of the OX system in the LH. We assessed *Snord116* expression in two different strains with OX deficiency, OX/ataxin-3 (Atx) mice and OX peptide knockout (KO) mice [9, 36], and we found that only Atx mice showed a significant increase in *Snord116*. This line selectively loses OX neurons and their co-transmitters. In contrast, in KO mice that do not display a loss of OX neurons but are lacking OX peptides, the level of *Snord116* was unaffected. The increase in *Snord116* in mice with depletion of OX neurons is probably a compensatory mechanism. These results also suggest the role of *Snord116,* a paternally imprinted gene in regulating the hypothalamus and the OX system. Our assumption is also supported by a recent study [48] that described the role of *Peg3* in the development and expression of OX and MCH neurons. Our study indicated that PEG3 is able to bind OX promotors by increasing the expression of OX. However, a reduced binding of PEG3 was observed in mutant mice relative to control mice, which may be explained by a reduction in OX neurons. Thus, *Peg3* was selectively altered in our PWScr$^{m+/p-}$ mutant mice as well as in narcoleptic mice. In particular, *Peg3* was found to be altered only in Atx narcoleptic mice, while it was unchanged in Ppox KO mice. This may be explained by the fact that PEG3 binds the OX promoter, which is not altered in KO mice because they have a null mutation. Our study suggests that these two paternally imprinted genes, *Snord116* and *Peg3*, are unlikely to interact with each other, however both contribute to the development and OX neurons. Indeed, in our *in vitro* experiment with immortalized hypothalamic cells, knockdown of *Snord116* did not directly change the levels of *Peg3*. These evidence are in line with the pioneering evidence in androgenetic mice [1] that paternal genome contains important contributions for the formation of the hypothalamus. In particular, our study implies that both *Snord116* and *Peg3* play a crucial role towards the formation of OX neurons. Therefore, this study advocates also for polygenic effect, the mechanism where multiple genes (e.g., imprinted genes) exerts effects on the same trait, perhaps across different conditions.

We observed that PWScr$^{m+/p-}$ mutant mice present a high body temperature coupled with an increase and lack of appropriate thermoregulatory responses. Thermoregulation is tightly integrated with the regulation of sleep and is also controlled by OX neuromodulation [37, 49]. For example, narcoleptic subjects exhibit a paradoxical lower core body temperature while awake [50] and a higher body temperature during sleep [51, 52]. In mammals, in physiological conditions, peripheral vasodilatation helps decrease the core body temperature during sleep initiation. Our mutant mice displayed a high body temperature during the light period, which corresponded to their resting phase/subjective sleep. Interestingly, narcoleptic mice show body similar temperature abnormalities [53]. Moreover, when PWS mutant mice were kept at the TNZ, where resting metabolic rate remains stable and where REM sleep is preferentially increased [54, 55], we observed a surprising thermoregulatory response coupled with an altered homeostatic REM sleep response. REM sleep did not increase, and the peripheral thermoregulatory response of the mutant mice resembled what would be expected in a sub-neutrality (e.g., 22°C) environment. REM sleep is a stage of sleep in which thermoregulation is suspended; for this reason, REM sleep expression is more sensitive to ambient temperature manipulation than NREM sleep [54, 55]. A recent study [56] described that endotherms have evolved neural circuits to opportunistically promote REM sleep when the need for thermoregulatory defense is minimized, such as in TNZ conditions, suggesting a tight link between thermoregulation and REM sleep. In our study, the increase in body weight observed at the TNZ suggests that thermoneutrality is a permissive condition that induces body weight gain but does not compensate for the metabolic abnormality in these mice. Indeed, the differences with wild-type mice remained unchanged. Mutants showed growth retardation at both environmental conditions investigated, namely, at both 22°C and 30°C.

The transcriptomic analysis suggests that loss of *Snord116* might promote inflammatory responses and negatively affect synaptic organization in the hypothalamus, as previously observed in post-mortem hypothalamic brain tissue from PWS patients [29]. Additionally, we observed that SD impacts significantly the transcriptome of the hypothalamus in mutant mice compared to control mice were only mild changes occur. Overall, the electrophysiological data together with the transcriptomic data suggest that loss of *Snord116* leads to impaired homeostatic response that negatively affects the biological processes of the hypothalamus and we observe that these effects are more pronounced in the context of SD. This data suggest that the sleep alterations observed in up to 76% of PWS patients [57, 58] represents a comorbidity that significantly affect the quality of life of these patients. Therefore, our results may provide compelling strategies to target dysregulated mechanisms in the hypothalamus of PWS patients affected by abnormal or poor sleep.

In conclusion, these new evidence are in agreement with pioneer studies in androgenetic chimeric mice [1], in which was suggested that the paternal genome may account for regulatory mechanisms in the hypothalamus. Moreover, it reinforce also the recent hypothesis that genomic imprinting plays a crucial role in mammalian sleep [3].

Methods:

Animal husbandry, breeding, and genotyping

All animals were housed in controlled temperature conditions (22 ± 1 °C) under a 12 h light/dark cycle (light on 08:00–20:00), with libitum access to food (standard chow diet) and water unless otherwise required by the experimental procedure.

Experiments were performed using adult mice at 15-17 weeks with paternal deletion of the *Snord116* gene and *IPW* exons A1/A2 B [17] (PWScr$^{m+/p-}$) and their wild-type littermates as control mice (PWScr$^{m+/p+}$). To maintain the colony, mice were bred and kept through paternal inheritance on a C57BL/6J background. Genotyping was performed as previously described [5]. Briefly, PCR analysis of genomic DNA from ear punches was performed using the primer pair PWScrF1/PWScrR2 (5'-AGAATCGCTTGAACCCAGGA and 5'-GAGAAGCCCTGTAACATGTCA, respectively). The deletion of PWScr resulted in a PCR product of approximately 300 bp, which was absent in the wild-type genotype.

For experiments in narcoleptic mice, 3 age-matched groups of male and female congenic mice from two different strains (≥ 9 generations of backcrossing) on the C57Bl/6J genetic background were used, as follows: (i) mice with congenital deficiency of OX gene (*Ppox*) knockout (KO) [9] (n=11); (ii) mice hemizygous for a transgene (ataxin-3 [Atx] mice), the targeted expression of which causes selective ablation of OX neurons [36] (n=4); and (iii) wild-type controls (n= 4). Mouse colonies were maintained in the facilities of the Department of Biomedical and NeuroMotor Sciences at the University of Bologna, Italy. Mice were housed under a 12-h light/dark cycle at an ambient temperature of 25°C with free access to water and food (4RF21 diet, Mucedola, Settimo Milanese, Italy).

All animal procedures were approved by the Animal Research Committee and the Veterinary Office of Italy for Istituto Italiano di Tecnologia (IIT) Genova. All efforts were made to minimize the number of animals used and any pain and discomfort according to the principles of the 3Rs [59].

Experimental approach

Neuronal activity in the mouse LH is time-locked with different behavioural and physiological states of the brain

To identify neuronal populations in the LH that control different physiological behaviours, we adopted a combined experimental approach (Figure 1A) in which we monitored single unit activity (SUA) at the LH in parallel with the cortical state of each animal by means of electroencephalogram and electromyogram (EEG/EMG) recordings. The EEG/EMG information allows the identification of wakefulness, REM sleep and NREM sleep states in the animal, which represent the three main behavioural states of the mammalian brain. Mice were kept throughout a regular sleep-wake cycle, and EEG/EMG/SUA were recorded during the light-to-dark transition (baseline 1, B1) and during the dark-to-light transition (baseline 2, B2) to test the neuronal responses during the minimum and maximum levels of sleep pressure, respectively (Figure 1B upper panel). Then, each mouse underwent sleep deprivation (SD) to test the homeostatic response following sleep loss (Figure 1B middle panel, see supplementary materials for the SD procedures). Moreover, to test the other fundamental function of LH, feeding, we food deprived each animal during the 12 h of darkness of the light/dark cycle, and then, when food was made available, we evaluated the neuronal responses to food intake (Figure 1B lower panel).

Experimental protocols

LH neuronal activity recordings

To investigate the neuronal dynamics of the lateral hypothalamus (LH), EEG/EMG and SUA were simultaneously recorded in eight male adult PWScr$^{m+/p-}$ and PWScr$^{m+/p+}$ mice. Animals were individually housed after surgery in their home cages with a food hopper (a hole with an infrared beam) connected to a food dispenser that automatically delivers food pellets after a nose poke (powered by AM-Microsystems [60]. The food used was 20 mg dustless precision pellets (Bioserv). After a 7-day recovery period after surgery, each mouse was connected to a flexible cable and swivel that allowed free movement within the cages; the mice were habituated for 2 days to the cable before SUA and EEG/EMG recordings (Figure 1A). Recordings of EEG/EMG with SUA were acquired at two different baseline (BL) time points (B1 and B2; Figure 1A) for 2 h according to the C Process and S Process of sleep. Next, to investigate sleep homeostasis, SUA and EEG/EMG were recorded during the first hour of the rebound period (RB, Figure 1A) following 6 h of total sleep deprivation (SD) and at other two time points over the 18-h recovery period (SD1 and SD2, Figure 1A).

After a restoration period of 5 days from the previous SD, animals were fasted for 12 h during the dark period, which corresponds to the active phase of mice. At the beginning of the light period, mice were fed. A few food pellets were initially provided to encourage the mice to eat, and thereafter, food pellets were provided only after nose-poke activity. SUA was continuously recorded for 2 h after being fed (Figure 1A). EEG/EMG was not recorded during this time. At the end of the last recording session, animals were sacrificed, and the locations of the recording electrodes were verified histologically (see the supplementary methods for the histology process)

Homeostatic investigation of sleep

To investigate the role of the *Snord116* gene in the regulation of the homeostatic component of sleep, we recorded EEG/EMG in ten male adult PWScr$^{m+/p-}$ and PWScr$^{m+/p+}$ mice over 24 h of baseline (BL) at 22 ± 1°C. The BL recordings began at ZT 0 (the time of light onset in the 12 h light/dark cycle), and then, mice were sleep deprived during the first 6 h of the light phase (ZT 0–6) by gentle handling (introduction of novel objects into the cage, tapping on the cage, and, when necessary, delicately touching) and then allowed 18 h of recovery (ZT 6–24, RB).

Homeostatic investigation of REM sleep

To investigate the REM sleep propensity, we housed male adult PWScr$^{m+/p-}$ and PWScr$^{m+/p+}$ mice for five weeks at 30 ± 1°C, which is close to or within the thermoneutral zone (TNZ) of mice [61, 62].

Then, these mice underwent continuous recordings for 24 h at 30°C ambient temperature while undisturbed and freely moving in their cages.

RNA sequencing and analysis

For this study the whole hypothalamus of both genotypes of mice were investigated: PWScr$^{m+/p-}$ mice and PWScr$^{m+/p+}$ mice at three different time points at ZT 0 (G1; PWS n=3 and WT n=3), immediately after 6-h of total SD (G2; PWS n=4 and WT n=4), and 1 h after previous SD (GT3; n=4). Total RNA was homogenized in Trizol Reagent (Sigma-Aldrich). Libraries were prepared using a TruSeq polyA mRNA kit (Illumina) according to the manufacturer's instructions and sequenced by using the NovaSeq 6000 System (Illumina). Raw sequence reads were quality controlled through FASTQC (https://www.bioinformatics.babraham.ac.uk/projects/fastqc/) and trimmed using Trimmomatic (v0.38) [63]. To quantify the transcript abundances, we used Kallisto (v0.44.0) [64]. Kallisto was also used to build an index from the mouse reference genome (EnsDb.Mmusculus.v79) with default parameters. To import and summarize transcript-level abundance of Kallisto, the R package Tximport was used. Differential expression was assessed using DSeq2 [65]. For false discovery rate correction, adjusted p-values less than 0.05 were selected, and only genes with > 2-fold change were considered in the analyses. The sequencing data are deposited in GEO accession number GSE139524.

GO analysis was performed using Metascape [66] (http://metascape.org/). The identified DEGs are listed in Tables S8 and S9. To compare mice and human DEGs in snord116 vs WT and PWS vs healthy controls, respectively, we run a homology analysis of the human DEGs toward the mice DEGs (non-coding RNAs were excluded from the analysis) and performed hypergeometric test. Significance of over-representation of GO terms was calculated using the hypergeometric test, corrected for multiple testing with a Benjamini & Hochberg false discovery rate correction [49], and a significance cut-off of 0.05 was applied to the result.

Electrophysiological data analysis

Cortical EEG/EMG signals were recorded using Dataquest A.R.T. (Data Science International). Signals were digitized at a sampling rate of 500 Hz with a filter cut-off of 50 Hz. EEG signals were filtered at 0.3 Hz (low-pass filter) and 0.1 KHz (high-pass filter). The polysomnographic recordings were visually scored offline using SleepSign software (Kissei Comtec Co. Ltd, Japan) per four second epoch window to identify wakefulness (W), NREM or REM sleep stages, as previously described [67, 68]. Scoring was performed by a single observer who was blinded to the mouse groups.

Specifically, W, NREM and REM states were scored when characteristic EEG/EMG activity occupied 75% of the epoch [67, 68]. EEG epochs determined to have artefact (interference caused by scratching, movement, eating, or drinking) were excluded from the analysis. Artefact comprised <5-8% of all recordings used for analysis.

The percentage of time spent in total sleep, NREM and REM sleep out of the total recording time was determined. The amount of time spent in each stage was established by counting the types of epochs (W or NR or R) and averaging over 2-h periods. The spectral characteristics of the EEG were further analysed. The EEG power densities of the delta (0, 5–4 Hz) and theta (5–9 Hz) frequencies in NREM and REM sleep were computed for all conditions investigated. The theta and delta power of each subject was normalized by the mean of the last 4-h of the light period. To exclude variability due to the implantation, the power density of each animal was normalized to the power density of the last 4-h of the light period of the 24-h recording (22°C and 30°C, respectively). The temperature was recorded at a sampling rate of 5 Hz within the range of 34°C – 41°C and averaged over 2-h periods. A two-way ANOVA with repeated measures (factors of group x time) was used for the statistical analysis of the 2-h averaged time-course changes in the percentage of each sleep stage (W, NREM and REM sleep), delta power, theta power and body temperature between the two genotypes ($^{+/+}$ vs. $^{-/-}$). The statistical analysis of the cumulative amount of W, NREM, and REM sleep over the dark and light periods among the groups at BL, after SD and at the TNZ was performed with one-way ANOVA. An unpaired t-test was used to compare differences in the sleep stages and in the delta and theta power during the first 4 h of rebound after SD between the two genotypes.

SUA data acquisition was performed using an RX7 system (Tucker Davis Technology, TDT). The synchronization between the behavioural set up and the TDT system was guaranteed with transistor-transistor logic (TTL) from the CHORA feeders to the TDT system. The data were digitally sampled at 12 kHz. To detect spike timestamps, the neural traces were filtered with a bandpass filter (300 – 5000 Hz), and then, the common average reference (CAR) was applied [69]. Spikes were detected using a hard threshold that was computed as previously described [70]. A correlation filter was applied between each detected spike and the corresponding signal chunk in the other recording sites to detect and exclude false positive spikes given by movement artefact.

To specifically identify active neurons in the LH, we imposed two criteria: (i) the refractory period following a spike was set to 1 ms; and (ii) the maximum duration of a waveform was set to 5 ms. Spikes of individual neurons were sorted offline using the noise robust LDA-GMM algorithm based on a linear discriminant analysis [71]. To identify neurons that specifically respond to a particular sleep-wake cycle, the unit activity was subsequently analysed per 4-s epoch in each sleep-wake stage for the average discharge rate (spikes per second). Classification of units according to the state in which their maximal discharge rate occurred was performed by ANOVA followed by post hoc paired t-tests with the Bonferroni correction, ($P < 0.05$)[72]. This analysis allowed the classification of units into three main neuronal populations that were shown to respond during specific sleep-wake stages (Figure 1B).

Moreover, to identify the neurons related to feeding behaviour in the LH, we assessed the firing rate of neurons that responded after the food was released by aligning the unit firing to the pellet release from the CHORA feeder after a spontaneous nose-poke activity. The mean baseline firing rate of each neuron was determined in the interval of 5 s before the pellet was released. Paired Student's t-tests were used to classify the firing rate differences of the same units before and after the food was released. To motivate the mice to perform more trials, they were food deprived for 12 h during the dark period, and the recording session started at the beginning of the light period for the following 2 h. Sessions were videotaped and reviewed to eliminate trials in which the mice performed the nose-poke activity but the food was not eaten. Video analysis also demonstrated that grooming rarely occurred and, thus, did not affect SUA. Indeed, grooming has been shown to induce moderate OX neuron activity [73]. Among all sessions, a mean of 3.25 ± 1.49 trials for the PWScr$^{m+/p-}$ mice and 2 ± 0.69 trials for the PWScr$^{m+/p-}$ mice were removed from the analysis because the food was not eaten.

Statistics

Values were tested for a Gaussian distribution with the Kolmogorov–Smirnov test. Data are presented as the mean ± standard error of the mean (SEM). Two-way repeated-measures analysis of variance (ANOVA) was used to perform group comparisons with multiple measurements. Paired and unpaired t tests were used for single value comparisons. One-way ANOVA was used to compare more than two groups, followed by post hoc Tukey's test. The Bonferroni correction was further applied in the post hoc analysis, as appropriate, to correct for multiple comparisons. Neuronal dynamics of the LH were analysed by the chi-square test. Phenopy [60] was used for sleep, temperature and SUA analyses, while GraphPad Prism6 (GraphPad Prism Software, Inc.) was used for statistical analysis. Type I error α was set to 0.05 ($p < 0.05$).

Study Approval

The study was approved by the ethics committee of the Italian Ministry of Healthy and subsequently approved by the ethics committee of the Italian institute of Technology (IIT) – Genova, Italy (n.089).

Author contributions

MP designed the study. MP, MF performed the animal experiments. VT provided infrastructural support. AF and MP performed and analysed the gene expression analysis. MP and MF performed the EEG and SUA analysis. AF performed the ChiP experiment. MC analysed data from the infrared thermocamera. AU and FK analysed the RNAseq data. EJH contributed resources. CB, LMV and ZG provided and dissected brain samples from narcoleptic mice. MP and VT drafted and finalized the manuscript. All authors revised and finalized it.

Acknowledgement

We thank Simone Bellini, a master student of Tucci's laboratory for her help with the RNA extraction and RT-qPCR.

References

1. Keverne, E.B., et al., *Genomic imprinting and the differential roles of parental genomes in brain development.* Brain Res Dev Brain Res, 1996. **92**(1): p. 91-100.
2. Bonnavion, P., et al., *Hubs and spokes of the lateral hypothalamus: cell types, circuits and behaviour.* J Physiol, 2016. **594**(22): p. 6443-6462.
3. Tucci, V., *Genomic Imprinting: A New Epigenetic Perspective of Sleep Regulation.* PLoS Genet, 2016. **12**(5): p. e1006004.
4. Tucci, V., et al., *Genomic Imprinting and Physiological Processes in Mammals.* Cell, 2019. **176**(5): p. 952-965.
5. Lassi, G., et al., *Deletion of the Snord116/SNORD116 Alters Sleep in Mice and Patients with Prader-Willi Syndrome.* Sleep, 2016. **39**(3): p. 637-44.
6. Holm, V.A., et al., *Prader-Willi syndrome: consensus diagnostic criteria.* Pediatrics, 1993. **91**(2): p. 398-402.
7. Swaab, D.F., *Prader-Willi syndrome and the hypothalamus.* Acta Paediatr Suppl, 1997. **423**: p. 50-4.
8. Vgontzas, A.N., et al., *Daytime sleepiness and REM abnormalities in Prader-Willi syndrome: evidence of generalized hypoarousal.* Int J Neurosci, 1996. **87**(3-4): p. 127-39.
9. Chemelli, R.M., et al., *Narcolepsy in orexin knockout mice: molecular genetics of sleep regulation.* Cell, 1999. **98**(4): p. 437-51.
10. Mignot, E., et al., *The role of cerebrospinal fluid hypocretin measurement in the diagnosis of narcolepsy and other hypersomnias.* Arch Neurol, 2002. **59**(10): p. 1553-62.
11. Omokawa, M., et al., *Decline of CSF orexin (hypocretin) levels in Prader-Willi syndrome.* Am J Med Genet A, 2016. **170A**(5): p. 1181-6.
12. Nevsimalova, S., et al., *Hypocretin deficiency in Prader-Willi syndrome.* Eur J Neurol, 2005. **12**(1): p. 70-2.
13. Adamantidis, A.R., et al., *Neural substrates of awakening probed with optogenetic control of hypocretin neurons.* Nature, 2007. **450**(7168): p. 420-4.
14. Schone, C. and D. Burdakov, *Orexin/Hypocretin and Organizing Principles for a Diversity of Wake-Promoting Neurons in the Brain.* Curr Top Behav Neurosci, 2017. **33**: p. 51-74.
15. Jego, S., et al., *Optogenetic identification of a rapid eye movement sleep modulatory circuit in the hypothalamus.* Nat Neurosci, 2013. **16**(11): p. 1637-43.
16. Seifinejad, A., et al., *Molecular codes and in vitro generation of hypocretin and melanin concentrating hormone neurons.* Proc Natl Acad Sci U S A, 2019.
17. Skryabin, B.V., et al., *Deletion of the MBII-85 snoRNA gene cluster in mice results in postnatal growth retardation.* PLoS Genet, 2007. **3**(12): p. e235.
18. Schoonakker, M., et al., *Heterogeneity in the circadian and homeostatic modulation of multiunit activity in the lateral hypothalamus.* Sleep, 2018. **41**(6).
19. Hassani, O.K., M.G. Lee, and B.E. Jones, *Melanin-concentrating hormone neurons discharge in a reciprocal manner to orexin neurons across the sleep-wake cycle.* Proc Natl Acad Sci U S A, 2009. **106**(7): p. 2418-22.
20. Polex-Wolf, J., et al., *Hypothalamic loss of Snord116 recapitulates the hyperphagia of Prader-Willi syndrome.* J Clin Invest, 2018. **128**(3): p. 960-969.
21. Qi, Y., et al., *Snord116 is critical in the regulation of food intake and body weight.* Sci Rep, 2016. **6**: p. 18614.
22. Amici, R., et al., *The influence of a heavy thermal load on REM sleep in the rat.* Brain Res, 1998. **781**(1-2): p. 252-8.
23. Amici, R., et al., *Cold exposure and sleep in the rat: REM sleep homeostasis and body size.* Sleep, 2008. **31**(5): p. 708-15.
24. Szymusiak, R. and E. Satinoff, *Maximal REM sleep time defines a narrower thermoneutral zone than does minimal metabolic rate.* Physiol Behav, 1981. **26**(4): p. 687-90.

25. Ehlen, J.C., et al., *Maternal Ube3a Loss Disrupts Sleep Homeostasis But Leaves Circadian Rhythmicity Largely Intact.* J Neurosci, 2015. **35**(40): p. 13587-98.
26. Huber, R., T. Deboer, and I. Tobler, *Effects of sleep deprivation on sleep and sleep EEG in three mouse strains: empirical data and simulations.* Brain Res, 2000. **857**(1-2): p. 8-19.
27. Li, P., et al., *Circadian blood pressure and heart rate rhythms in mice.* Am J Physiol, 1999. **276**(2): p. R500-4.
28. Kozlov, S.V., et al., *The imprinted gene Magel2 regulates normal circadian output.* Nat Genet, 2007. **39**(10): p. 1266-72.
29. Bochukova, E.G., et al., *A Transcriptomic Signature of the Hypothalamic Response to Fasting and BDNF Deficiency in Prader-Willi Syndrome.* Cell Rep, 2018. **22**(13): p. 3401-3408.
30. Zhou, Y., et al., *Metascape provides a biologist-oriented resource for the analysis of systems-level datasets.* Nat Commun, 2019. **10**(1): p. 1523.
31. Thiaville, M.M., et al., *DNA-binding motif and target genes of the imprinted transcription factor PEG3.* Gene, 2013. **512**(2): p. 314-20.
32. Kuroiwa, Y., et al., *Peg3 imprinted gene on proximal chromosome 7 encodes for a zinc finger protein.* Nat Genet, 1996. **12**(2): p. 186-90.
33. Moriguchi, T., et al., *The human prepro-orexin gene regulatory region that activates gene expression in the lateral region and represses it in the medial regions of the hypothalamus.* J Biol Chem, 2002. **277**(19): p. 16985-92.
34. Ye, A., H. He, and J. Kim, *PEG3 binds to H19-ICR as a transcriptional repressor.* Epigenetics, 2016. **11**(12): p. 889-900.
35. Bogliotti, Y.S. and P.J. Ross, *Mechanisms of histone H3 lysine 27 trimethylation remodeling during early mammalian development.* Epigenetics, 2012. **7**(9): p. 976-81.
36. Hara, J., et al., *Genetic ablation of orexin neurons in mice results in narcolepsy, hypophagia, and obesity.* Neuron, 2001. **30**(2): p. 345-54.
37. Kuwaki, T., *Thermoregulation under pressure: a role for orexin neurons.* Temperature (Austin), 2015. **2**(3): p. 379-91.
38. McVea, S., et al., *Thermal dysregulation in Prader-Willi syndrome: a potentially fatal complication in adolescence, not just in infancy.* BMJ Case Rep, 2016. **2016**.
39. de Smith, A.J., et al., *A deletion of the HBII-85 class of small nucleolar RNAs (snoRNAs) is associated with hyperphagia, obesity and hypogonadism.* Hum Mol Genet, 2009. **18**(17): p. 3257-65.
40. Sahoo, T., et al., *Prader-Willi phenotype caused by paternal deficiency for the HBII-85 C/D box small nucleolar RNA cluster.* Nat Genet, 2008. **40**(6): p. 719-21.
41. Ding, F., et al., *SnoRNA Snord116 (Pwcr1/MBII-85) deletion causes growth deficiency and hyperphagia in mice.* PLoS One, 2008. **3**(3): p. e1709.
42. Miller, J.L., et al., *Nutritional phases in Prader-Willi syndrome.* Am J Med Genet A, 2011. **155A**(5): p. 1040-9.
43. Naganuma, F., et al., *Melanin-concentrating hormone neurons contribute to dysregulation of rapid eye movement sleep in narcolepsy.* Neurobiol Dis, 2018. **120**: p. 12-20.
44. Burdakov, D., M.M. Karnani, and A. Gonzalez, *Lateral hypothalamus as a sensor-regulator in respiratory and metabolic control.* Physiol Behav, 2013. **121**: p. 117-24.
45. Barson, J.R., I. Morganstern, and S.F. Leibowitz, *Complementary roles of orexin and melanin-concentrating hormone in feeding behavior.* Int J Endocrinol, 2013. **2013**: p. 983964.
46. Gonzalez, J.A., et al., *Inhibitory Interplay between Orexin Neurons and Eating.* Curr Biol, 2016. **26**(18): p. 2486-2491.
47. Manzardo, A.M., et al., *Higher plasma orexin A levels in children with Prader-Willi syndrome compared with healthy unrelated sibling controls.* Am J Med Genet A, 2016. **170**(8): p. 2097-102.

48. Seifinejad, A., et al., *Molecular codes and in vitro generation of hypocretin and melanin concentrating hormone neurons.* Proc Natl Acad Sci U S A, 2019. **116**(34): p. 17061-17070.
49. Cerri, M., et al., *Enhanced slow-wave EEG activity and thermoregulatory impairment following the inhibition of the lateral hypothalamus in the rat.* PLoS One, 2014. **9**(11): p. e112849.
50. Fronczek, R., et al., *Manipulation of core body and skin temperature improves vigilance and maintenance of wakefulness in narcolepsy.* Sleep, 2008. **31**(2): p. 233-40.
51. Mosko, S.S., J.B. Holowach, and J.F. Sassin, *The 24-hour rhythm of core temperature in narcolepsy.* Sleep, 1983. **6**(2): p. 137-46.
52. Pollak, C.P. and D.R. Wagner, *Core body temperature in narcoleptic and normal subjects living in temporal isolation.* Pharmacol Biochem Behav, 1994. **47**(1): p. 65-71.
53. Mochizuki, T., et al., *Elevated body temperature during sleep in orexin knockout mice.* Am J Physiol Regul Integr Comp Physiol, 2006. **291**(3): p. R533-40.
54. Parmeggiani, P.L., *Thermoregulation and sleep.* Front Biosci, 2003. **8**: p. s557-67.
55. Cerri, M., et al., *REM Sleep and Endothermy: Potential Sites and Mechanism of a Reciprocal Interference.* Front Physiol, 2017. **8**: p. 624.
56. Komagata, N., et al., *Dynamic REM Sleep Modulation by Ambient Temperature and the Critical Role of the Melanin-Concentrating Hormone System.* Curr Biol, 2019. **29**(12): p. 1976-1987 e4.
57. Gunay-Aygun, M., et al., *The changing purpose of Prader-Willi syndrome clinical diagnostic criteria and proposed revised criteria.* Pediatrics, 2001. **108**(5): p. E92.
58. Williams, K., et al., *Sleepiness and sleep disordered breathing in Prader-Willi syndrome: relationship to genotype, growth hormone therapy, and body composition.* J Clin Sleep Med, 2008. **4**(2): p. 111-8.
59. Tornqvist, E., et al., *Strategic focus on 3R principles reveals major reductions in the use of animals in pharmaceutical toxicity testing.* PLoS One, 2014. **9**(7): p. e101638.
60. Balzani, E., et al., *An approach to monitoring home-cage behavior in mice that facilitates data sharing.* Nat Protoc, 2018. **13**(6): p. 1331-1347.
61. Swoap, S.J., J.M. Overton, and G. Garber, *Effect of ambient temperature on cardiovascular parameters in rats and mice: a comparative approach.* Am J Physiol Regul Integr Comp Physiol, 2004. **287**(2): p. R391-6.
62. Speakman, J.R. and J. Keijer, *Not so hot: Optimal housing temperatures for mice to mimic the thermal environment of humans.* Mol Metab, 2012. **2**(1): p. 5-9.
63. Bolger, A.M., M. Lohse, and B. Usadel, *Trimmomatic: a flexible trimmer for Illumina sequence data.* Bioinformatics, 2014. **30**(15): p. 2114-20.
64. Bray, N.L., et al., *Near-optimal probabilistic RNA-seq quantification.* Nat Biotechnol, 2016. **34**(5): p. 525-7.
65. Love, M.I., W. Huber, and S. Anders, *Moderated estimation of fold change and dispersion for RNA-seq data with DESeq2.* Genome Biol, 2014. **15**(12): p. 550.
66. Tripathi, S., et al., *Meta- and Orthogonal Integration of Influenza "OMICs" Data Defines a Role for UBR4 in Virus Budding.* Cell Host Microbe, 2015. **18**(6): p. 723-35.
67. Pace, M., et al., *Role of REM Sleep, Melanin Concentrating Hormone and Orexin/Hypocretin Systems in the Sleep Deprivation Pre-Ischemia.* PLoS One, 2017. **12**(1): p. e0168430.
68. Pace, M., et al., *Rapid eye movements sleep as a predictor of functional outcome after stroke: a translational study.* Sleep, 2018. **41**(10).
69. Ludwig, K.A., et al., *Using a common average reference to improve cortical neuron recordings from microelectrode arrays.* J Neurophysiol, 2009. **101**(3): p. 1679-89.
70. Erickson, J.C., et al., *Falling-edge, variable threshold (FEVT) method for the automated detection of gastric slow wave events in high-resolution serosal electrode recordings.* Ann Biomed Eng, 2010. **38**(4): p. 1511-29.

71. Keshtkaran, M.R. and Z. Yang, *Noise-robust unsupervised spike sorting based on discriminative subspace learning with outlier handling.* J Neural Eng, 2017. **14**(3): p. 036003.
72. Lee, M.G., O.K. Hassani, and B.E. Jones, *Discharge of identified orexin/hypocretin neurons across the sleep-waking cycle.* J Neurosci, 2005. **25**(28): p. 6716-20.
73. Mileykovskiy, B.Y., L.I. Kiyashchenko, and J.M. Siegel, *Behavioral correlates of activity in identified hypocretin/orexin neurons.* Neuron, 2005. **46**(5): p. 787-98.

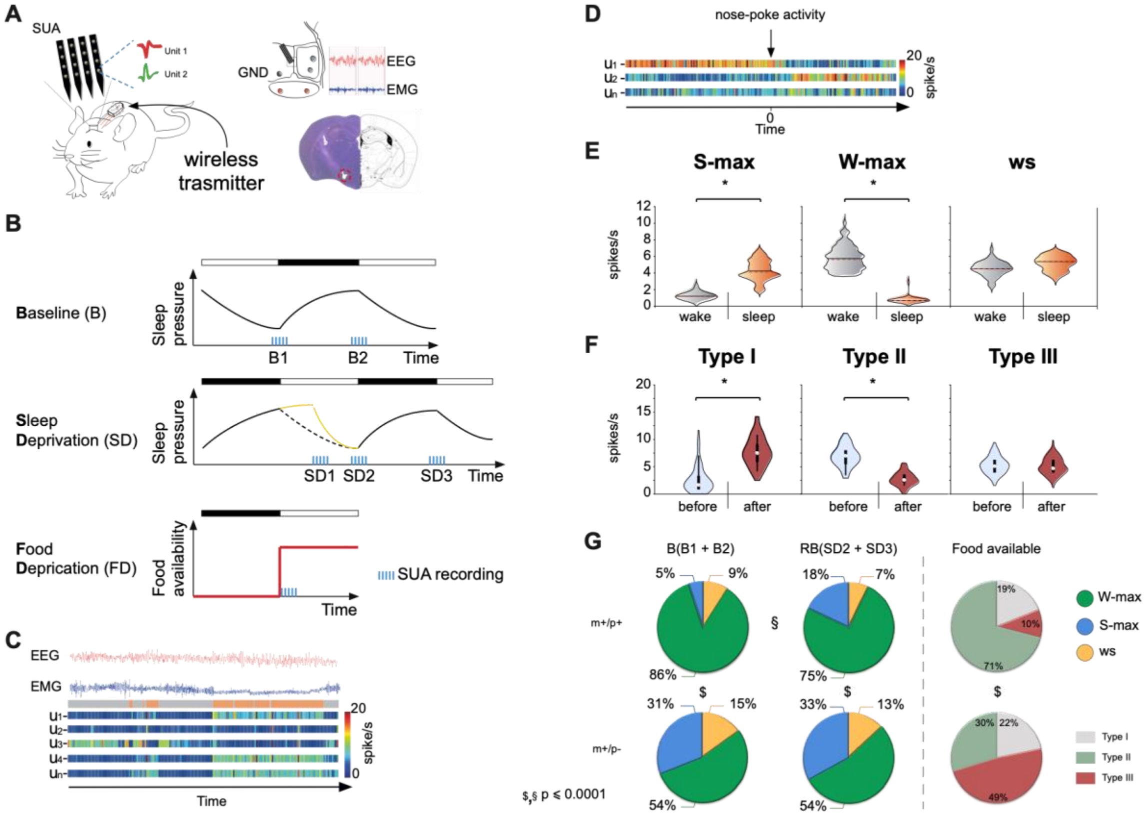

Figure 1

Figure 1 Loss of paternal *Snord116* alters neuronal dynamics in the LH associated with sleep and food. A) The cartoon shows mice chronically implanted with a microwire array of 16 channels and with an EEG-EMG wireless transmitter. The correct placement of the SUA electrode was histologically verified by 40-µm Nissl-stained coronal brain sections (bregma –1.10/–1.90). **B)** The experimental design used to record SUA and the sleep-wake cycle (see Methods). **C)** An example of sleep stages (i.e wakefulness in grey, sleep, including both NREM and REM sleep stages, in orange) aligned with the firing rate recorded in the LH. The heatmaps show the response firing rate in spikes/second from 0 Hz (blue) to 20 Hz (red). **D)** The heatmaps show the response firing rate used to classify neurons before and after food consumption (firing rate in spikes/second from 0 Hz [blue] to 20 Hz [red]). **E)** Violin plots of classified units according to the sleep-wake cycle according to ANOVA followed by post hoc Bonferroni correction ($p < .05$), see Methods. **F)** Violin plots of classified units according to their discharge related to food consumption (paired Student’s t-test of the firing rate between before and after the pellet was released, binned at 50 ms, $p < 0.05$), see Methods. **G)** The pie chart represents the distribution of recorded neurons according to the sleep-wake stage: wake (W-max, in green), sleep (both NREM and REM sleep, S-max, in blue) and not responding (ws, yellow). Food-related neurons are classified as Type I neurons, in grey; Type II neurons In green; Type III neurons, in red, see Methods. Differences between the two genotypes are indicated by $, while differences within groups across time points are indicated by §. Significance was computed with the chi-square test; for details on the statistical analysis, see Table S2, S3, and S4. The two genotypes investigated were PWScr$^{m+/p-}$ mice (n=4) and PWScr$^{m+/p+}$ mice (n= 4).

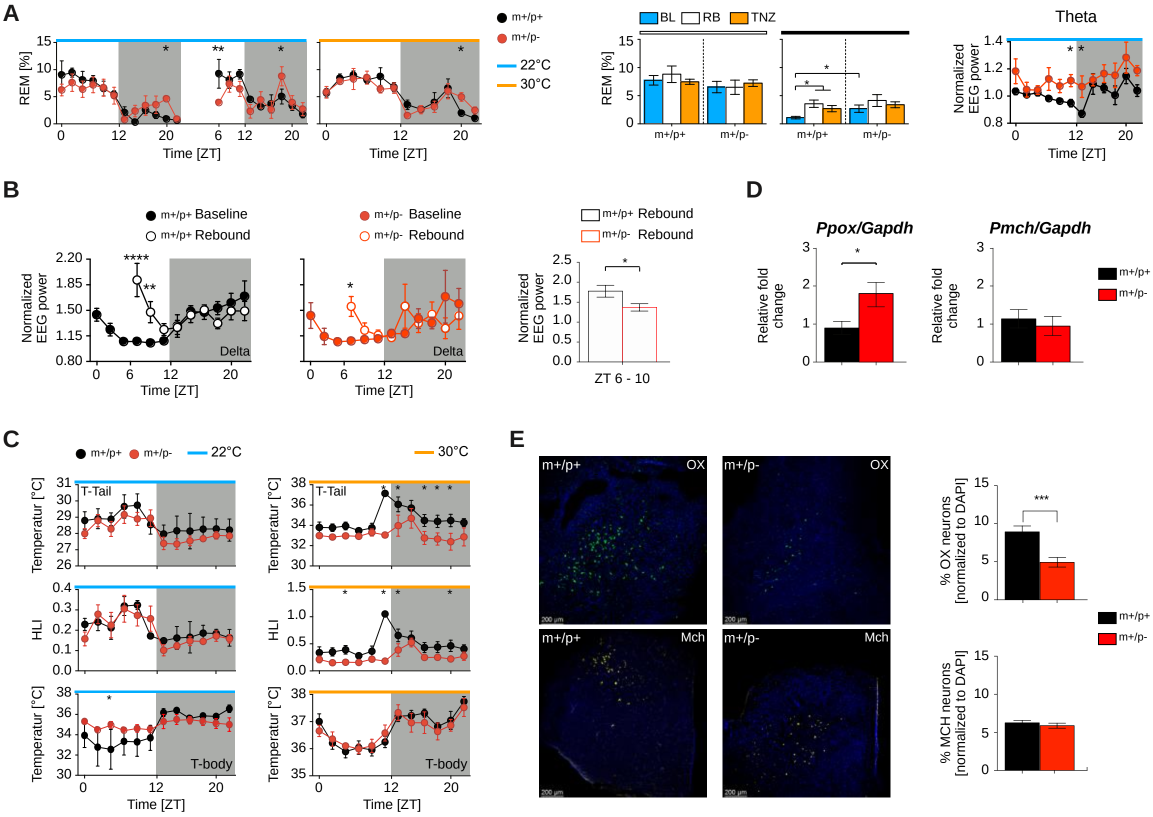

Figure 2

Figure 2

***Snord116* influenced REM sleep and its homeostatic regulation, thermoregulatory response via the orexin system**. **A)** Left panel shows the REM sleep distribution over 24-h period 1(2-h light/dark cycle) accounting for the baseline values (BL) and for the following 18-h after total SD accounting for the rebound period (RB). PWScr$^{m+/p-}$ (red) PWScr$^{m+/p-}$ (black) were recorded at 22°C (cyan bar) or at 30° C (orange bar). REM sleep was significantly altered in mutant mice relative to control mice at baseline and over the recovery period following 6-h of SD (two-way ANOVA: F (20, 160) = 8.66 p= <0.0001; “time”; F (8, 160) = 3.33; p= <0.001; “genotypes”), as well as at TNZ (two-way ANOVA: F (11, 88) = 11.61 p= <0.0001; “time”). Data are reported as the percentage in 2h bins, averaged within genotypes. Middle panel, the cumulative amount of REM sleep during the 12-h of the light period and dark period for mice recorded at 22°C (BL) in blue, after 6-h of SD over the rebound period (RB) in white and at 30°C (TNZ) in orange. During the dark period, PWScr$^{m+/p-}$ mice showed an increase in REM sleep (F(1.85, 4.74)= 18.06, p = .0082). Student’s unpaired t-test between genotypes indicates an increase in REM sleep in PWScr$^{m+/p-}$ mutant mice relative to PWScr$^{m+/p+}$ mice (t(8) = 2.30, p = .04). The right panel shows the spectral analysis. Theta power at 22°C between genotypes. Theta power during REM sleep was increased in PWScr$^{m+/p-}$ mice (two-way ANOVA:, F(11,88)= 3.08, p = <.001 “time”; F(1,8)= 8.04, p= .02 “genotypes”). **B)** The panel shows the delta power at 22°C between baseline vs rebound for both genotypes. Wild-type mice displayed a significant increase in delta power following SD from ZT6 to ZT10 (two-way ANOVA: F(11,88)= 28,77 p= <0.0001 “interaction”), while mutant mice showed a mild increase only at ZT 6 (two-way ANOVA: F(11,88)= 12,25 p= <0.0001 “interaction”). Right panel, the average of the first 4-h of recovery after SD between the two genotypes for the delta power. PWScr$^{m+/p-}$ mice showed lower delta than PWScr$^{m+/p+}$ mice (unpaired t-test: t(8) = 2.31, p = .04). Two genotypes were investigated: PWScr$^{m+/p-}$ mice (n= 10, 5 mice at 22°C and 5 mice at 30°C) and PWScr$^{m+/p+}$ mice (n= 10, 5 mice at 22°C and 5 mice at 30°C). **C)** Temperature profile for PWScr$^{m+/p+}$ and PWScr$^{m+/p-}$. The panel shows the T-tail, Heat loss index (HLI) and body temperature profiles recorded with an infrared thermocamera over 24-h. Recordings were performed under two different environmental conditions: at 22°C and at TNZ. Values are expressed as a 2-h mean ± SEM. PWScr$^{m+/p-}$ mice showed an increase in body temperature during the light period at ZT 6 at 22°C (two-way ANOVA: $F(11,88)= 3.53$, $p = .0004$ "time"; $F(11,88)= 7.86$, $p = <.0001$ "genotypes"). At 30°C, T-tail (two-way ANOVA: $F(11,88)= 2.68$, $p = <.0001$; "interaction") and HLI (two-way ANOVA: main effect of time-of-day, $F(11,88)= 4.72$, $p = <.0001$ "interaction") were increased in PWScr$^{m+/p+}$ mice relative to mutant mice. Two genotypes were investigated: PWScr$^{m+/p-}$ mice (n= 10, 5 mice at 22°C and 5 mice at 30°C) and PWScr$^{m+/p+}$ mice (n= 10, 5 mice at 22°C and 5 mice at 30°C). **D)** *Ppox* and *Pmch* gene expression analysis in PWScr$^{m+/p-}$ mice versus controls. PWScr$^{m+/p-}$ mice (red bar) showed an increase in *Ppox* (unpaired t-test: $t(8) = 2.49$, $p = .03$) compared with PWScr$^{m+/p+}$ mice (black bar). See supplementary methods. **E)** Cell count distribution of OX immunoreactive neurons (upper) and MCH immunoreactive neurons (below) in the lateral hypothalamus of PWScr$^{m+/p-}$ mice (right) versus controls (left). Coronal sections were stained with OX- and MCH-specific antibodies, counterstained with DAPI and scored. Two genotypes were investigated: PWScr$^{m+/p-}$ mice (n=4) and PWScr$^{m+/p+}$ mice (n= 4). The number of OX^{+} neurons was reduced in the PWScr$^{m+/p-}$ mouse group (unpaired t-test: $t(33) = 3.85$, $p = .0005$). See supplementary methods. Values are expressed as the percentage of positive neurons relative to all stained nuclei (mean ± SEM). Asterisks (*) indicate a significant difference between genotypes: * $P \leq .05$; ** $p \leq .01$; *** $p \leq .001$; **** $p \leq .0001$.

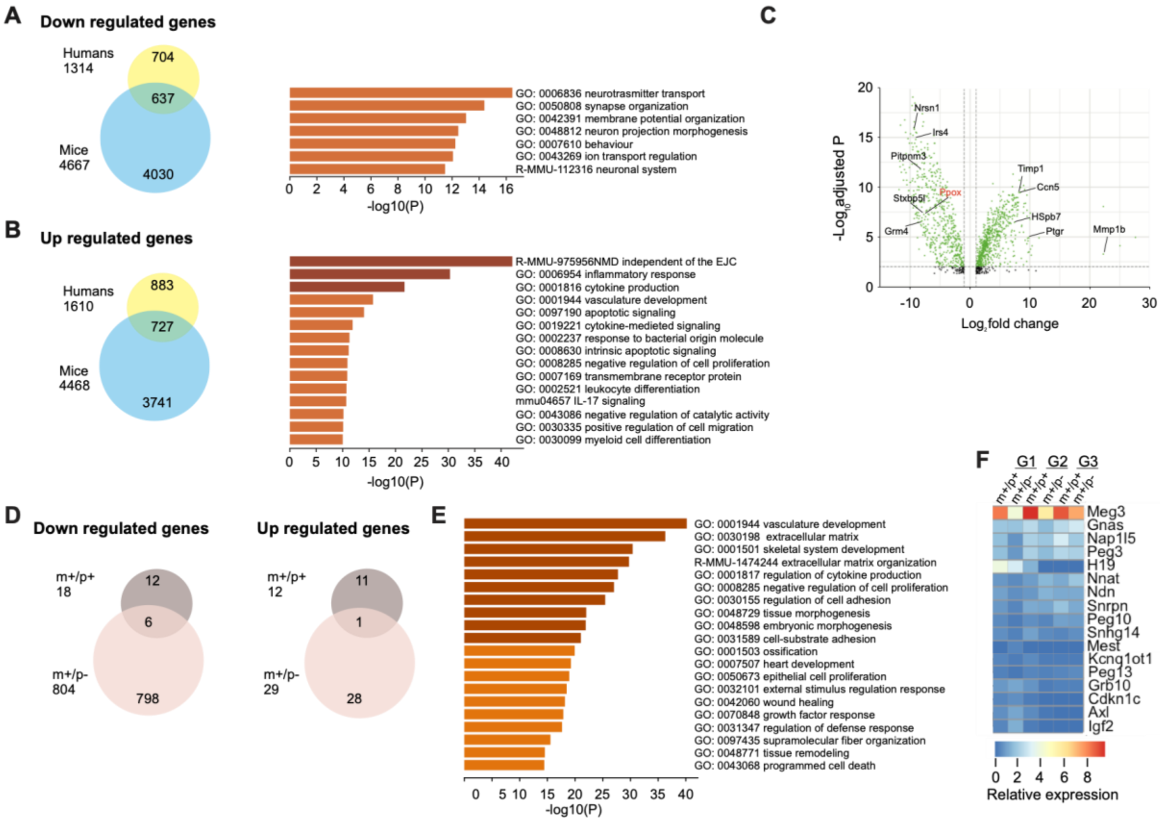

Figure 3

Figure 3

***Snord116* loss significantly impacts molecular machinery in the hypothalamus**. **A-B)** Venn diagrams illustrating the number of differentially expressed genes (DEGs) that are down- (A) and upregulated (B) in the hypothalamus of Prader–Willi syndrome (PWS) PWScr$^{m+/p-}$ mice relative to control mice and that overlap in human patients (according to [29]. The results of gene ontology (GO) enrichment analysis of biological processes for the overlapping DEGs are also shown in both A and B. **C)** Volcano plots of 637 and 727 DEGs in PWScr$^{m+/p-}$ mice in group 1 (G1; non-sleep deprived). **D)** Significantly down- and upregulated genes in the hypothalamus of PWScr$^{m+/p-}$ mutant mice compared with PWScr$^{m+/p+}$ control mice affected by sleep deprivation (G2 vs G3). **E)** GO enrichment analysis of biological processes for 833 (804 down- and 29 upregulated genes in panel D) DEGs in PWScr$^{m+/p-}$mutant mice that are significantly affected by sleep deprivation. **F)** Heatmap of the relative expression of imprinted genes common in humans and mice assessed in PWScr$^{m+/p-}$ mutant mice compared with the PWScr$^{m+/p+}$ mice in G1, G2 and G3. See also Tables S8 and S9. PWScr$^{m+/p-}$ mice and PWScr$^{m+/p+}$ mice at three different time points at ZT 0 (G1; PWS n=3 and WT n=3), immediately after 6-h of total SD (G2; PWS n=4 and WT n=4), and 1 h after previous SD (GT3; n=4).

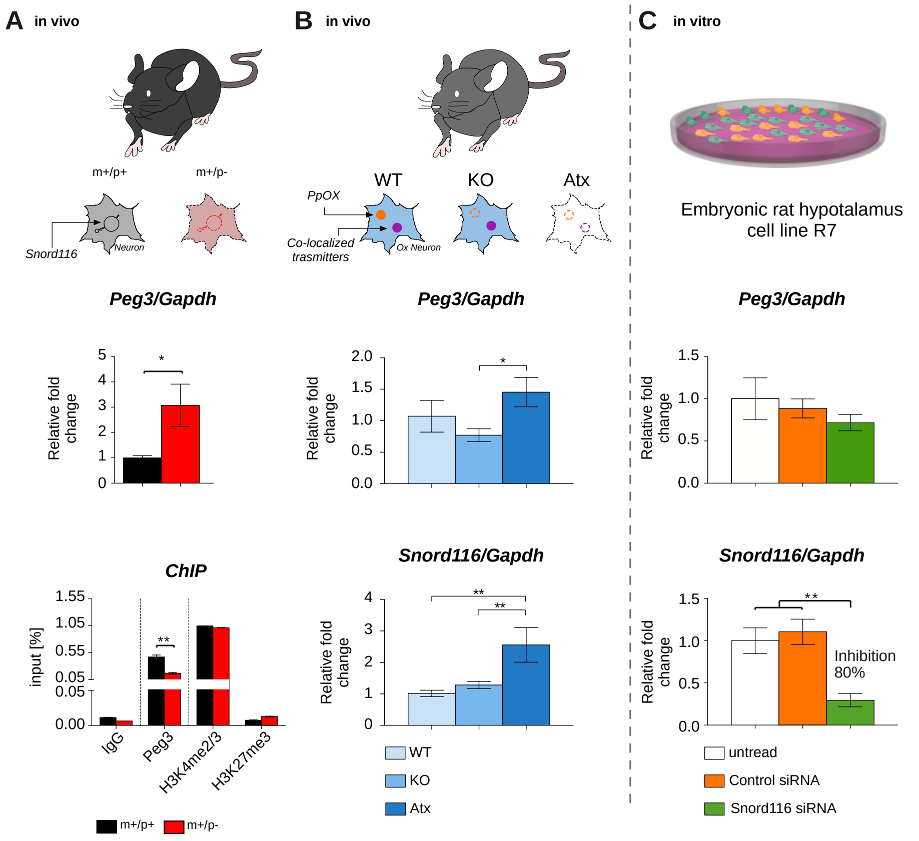

Figure 4

Figure 4

***Snord116* and *Peg3* play roles in the formation and maintenance of OX neurons**. *Peg3* regulates orexin expression in an independent manner from paternal *Snord116*. **A)** Upper panel, the gene expression analysis of *Peg3* in PWScr$^{m+/p-}$ mice (red) versus controls (black). *Peg3* mRNA assessed by qRT-PCR was significantly increased in PWScr$^{m+/p-}$ mice compared with PWScr$^{m+/p+}$ mice (unpaired t-test: t(6) = 2.45, p = .04). Values expressed are relative to the wild-type control mean ± SEM. *Gapdh* was used as a housekeeping gene; See supplementary methods. Bottom panel, ChIP analysis of PEG3 binding to the *Ppox* promoter region in PWScr$^{m+/p-}$ mice (red) versus controls (black). PEG3 binding was lower in PWScr$^{m+/p-}$ mice than in PWScr$^{m+/p+}$ mice (unpaired t-test: t(2) = 7.11, p = .01). See supplementary methods. **B)** *Peg3* gene expression (upper panel) and *Snord116* gene expression (bottom panel) in *Ppox* knockout (KO) and orexin neuron-ablated (ataxin-3 [Atx] mice). One-way ANOVA indicated that *Peg3* was significantly increased in Atx mice relative to KO mice, (F(2,16)= 0.02, Bonferroni post hoc test p = .03). Snord116 was increased in Atx mice relative to KO and control mice (WT) (one-way ANOVA F(2,16)= 3.50, Bonferroni post hoc test p = .002). The following genotypes of narcoleptic mice were investigated: WT (n=4), KO (n= 12) and Atx (n=4). **C)** *Snord116* and *Peg3* gene expression analysis in the *Snord116*-siRNA-treated immortalised hypothalamic rat cell line. *Snord116*-siRNA (green bars) reduced the expression of the *Snord116* gene compared with untreated cells or scrambled siRNA-treated cells (white and orange bars) (one-way ANOVA: F(2, 6)= 11.36, Bonferroni post hoc test p = .009). *Peg3* mRNA levels were unchanged, similar to *Snord116*-SiRNA, in untreated cells and scrambled siRNA-treated cells. The experiment was conducted in triplicate. Data are presented as the mean ± SEM. Asterisks (*) indicate a significant difference between genotypes: * P ≤ .05; **p ≤ .01; *** p ≤ .001; **** p ≤ .0001.